Electronic Supplementary Material

Multi arm quinoxaline-based acceptors formed by π-conjugation extension for efficient organic solar cells

Xinya Ran,[a,b] Dingding Qiu,[a] Yanan Shi,[c] Hao Zhang, [a] Jianqi Zhang,[a] Zhixiang Wei,*[a,b] Kun Lu*[a,b]

[a] *CAS Key Laboratory of Nanosystem and Hierarchical Fabrication, National Center for Nanoscience and Technology, Beijing 100190, China*

[b] *Sino-Danish Center for Education and Research, Sino-Danish College, University of Chinese Academy of Sciences, Beijing 100049, China*

[c] *National Engineering Research Center for Rare Earth, Grirem Advanced Materials Co., Ltd., Beijing 100088, China*

E-mail: lvk@nanoctr.cn; weizx@nanoctr.cn

1. Synthesis of FQx-IC and TQx-IC.

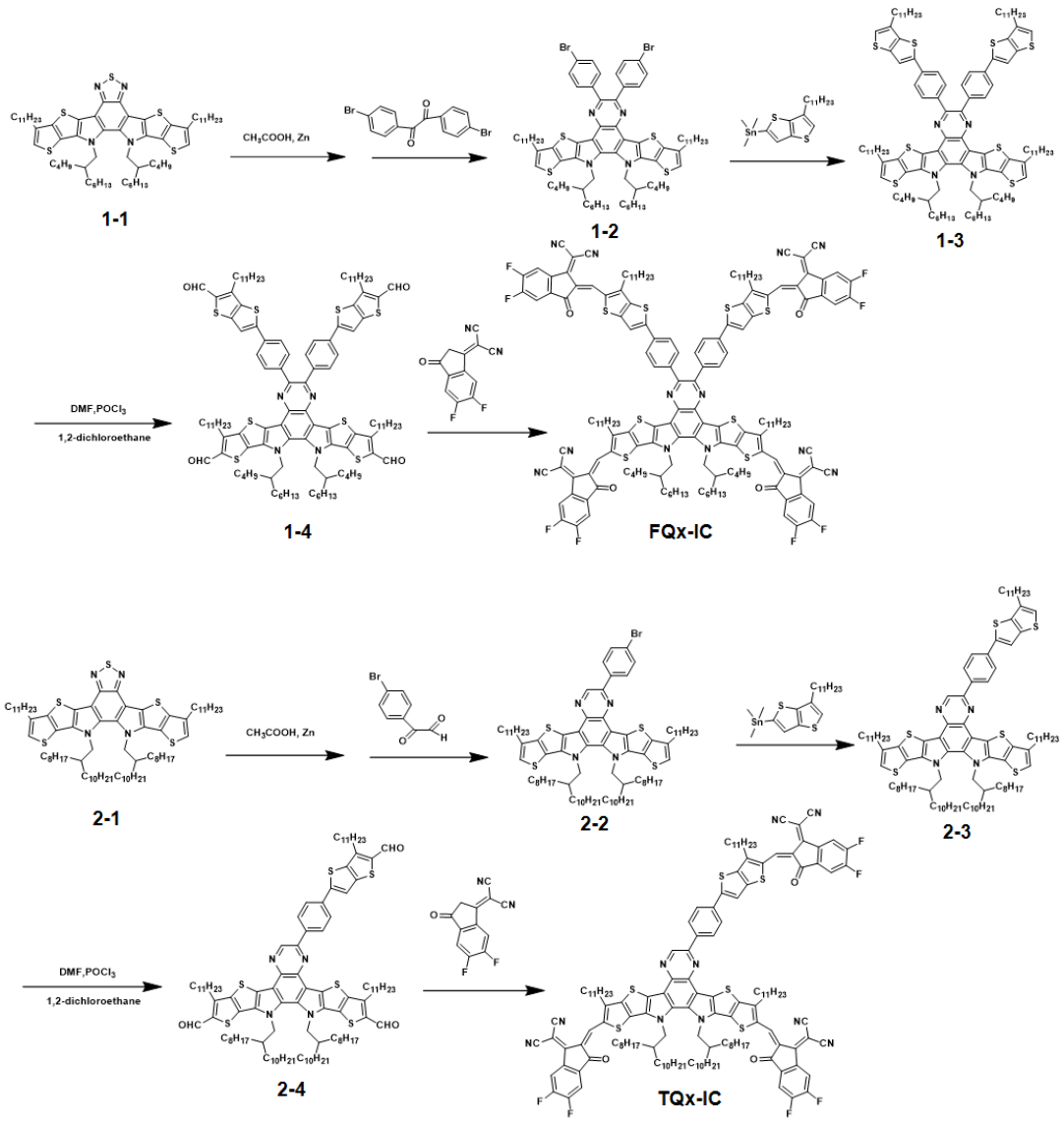

Scheme S1 Synthetic routes of FQx-IC and TQx-IC

The chemical name of materials:

FQx-IC: 2,2'-((2Z,2'Z)-((((13,14-bis(2-butyloctyl)-2,11-bis(((Z)-1 (dicyanomethylene)-5,6-difluoro-3-oxo-1,3-dihydro-2H-inden-2-ylidene)methyl)3,10-diundecyl-13,14 dihydrothieno[2",3":4',5']thieno[2',3':4,5]pyrrolo[3,2f]thieno [2",3":4',5'] thieno[2',3':4,5]pyrrolo[2,3-h]quinoxaline-6,7-diyl)bis(4,1phenylene))bis (3-undecyl thieno[3,2-b]thiophene-5,2-diyl))bis(methaneylylidene))bis(5,6-difluoro-3-oxo-2,3-dihydro-1H-indene-2,1-diylidene))dimalononitrile

TQx-IC: 2,2'-((2Z,2'Z)-((6-(4-(5-(((Z)-1-(dicyanomethylene)-5,6-difluoro-3-oxo-1,3-dihydro-2H-inden-2-ylidene)methyl)-6-undecylthieno[3,2-b]thiophen-2-yl)phenyl)-13,14-bis(2-octyldodecyl)-3,10-diundecyl-13,14 dihydrothieno[2",3":4',5']thieno [2',3':4,5]pyrrolo[3,2f]thieno[2",3":4',5']thieno[2',3':4,5]pyrrolo[2,3-h]quinoxaline-2,11-diyl)bis(methaneylylidene))bis(5,6-difluoro-3-oxo-2,3-dihydro-1H-indene-2,1-diylidene))dimalononitrile

Compound 1-1: 12,13-bis(2-butyloctyl)-3,9-diundecyl-12,13-dihydro- [1,2,5] thiadia zolo[3,4-e] thieno [2",3":4',5'] thieno [2',3':4,5] pyrrolo[3,2-g] thieno [2',3':4,5] thieno[3,2-b] indole

Compound 1-2：6,7-bis(4-bromophenyl)-13,14-bis(2-butyloctyl)-3,10-diundecyl-13, 14dihydrothieno [2",3":4',5'] thieno [2',3':4,5] pyrrolo [3,2f] thieno [2",3":4',5'] thieno [2',3':4,5] pyrrolo[2,3-h] quinoxaline

Compound 1-3: 13,14-bis(2-butyloctyl)-3,10-diundecyl-6,7-bis (4-(6-undecylthieno [3,2-b] thiophen-2-yl) phenyl)-13,14-dihydrothieno [2",3":4',5'] thieno [2',3':4,5] pyrrolo[3,2-f] thieno [2",3":4',5'] thieno [2',3':4,5] pyrrolo[2,3-h] quinoxaline

Compound 1-4: 13,14-bis(2-butyloctyl)-6,7-bis(4-(5-formyl-6-undecylthieno[3,2-b] thiophen-2-yl) phenyl)-3,10-diundecyl-13,14 dihydrothieno [2",3":4',5'] thieno [2',3':4,5] pyrrolo[3,2-f] thieno [2",3":4',5'] thieno [2',3':4,5] pyrrolo[2,3-h] quinoxaline-2,11-dicarbaldehyde

Compound 2-1: 12,13-bis(2-octyldodecyl)-3,9-diundecyl-12,13-dihydro- [1,2,5] thiadiazolo[3,4-e] thieno [2",3":4',5'] thieno [2',3':4,5] pyrrolo[3,2-g] thieno [2',3':4,5] thieno[3,2-b] indole

Compound 2-2: 6-(4-bromophenyl)-13,14-bis(2-octyldodecyl)-3,10-diundecyl-13,14-dihydrothieno [2",3":4',5'] thieno [2',3':4,5] pyrrolo [3,2 f] thieno [2",3":4',5'] thieno[2',3':4,5]pyrrolo [2,3-h] quinoxaline

Compound 2-3: 13,14-bis(2-octyldodecyl)-3,10-diundecyl-6-(4-(6undecylthieno[3,2-b] thiophen-2-yl) phenyl)-13,14-dihydrothieno [2",3":4',5'] thieno [2',3':4,5] pyrrolo

[3,2-f] thieno [2",3":4',5'] thieno [2',3':4,5] pyrrolo [2,3-h] quinoxaline

Compound 2-4: 6-(4-(5-formyl-6-undecylthieno[3,2-b] thiophen-2-yl) phenyl)-13,14 bis(2-octyldodecyl)-3,10-diundecyl13,14dihydrothieno [2",3":4',5'] thieno [2',3':4,5] pyrrolo [3,2f] thieno [2",3":4',5'] thieno [2',3':4,5] pyrrolo [2,3-h] quinoxaline-2,11-dicarbaldehyde

Compound 1-2：To a solution of compound 1-1 (600 mg, 0.56 mmol) in acetic acid (50 mL) was added zinc powder (728 mg, 11.2 mmol) in one portion. Then the mixture solution was heated to 90 °C for 5 h. After the solution was cooled to room temperature, the solid was removed by filtration. Transfer the filtrate to a three-tip flask containing 1,2-bis(4-bromophenyl)ethane-1,2-dione (309.1 mg, 0.84 mmol), then the mixture solution was heated to 110 °C for 20 h. After cooling to room temperature, the mixture was washed with saturated salt water and extracted with methylene chloride. The solvent was removed under reduced pressure. The crude product was subsequently purified by column chromatography on silica gel to afford compound 1-3 as yellow oily solid (300 mg, 50% yield). ^{1}H NMR (400 MHz, $CDCl_3$) δ 7.87 (d, J = 8.2 Hz, 4H), 7.66 (d, J = 6.4 Hz, 4H), 6.90 (s, 2H), 4.39 (d, J = 7.2 Hz, 4H), 2.73 (d, J = 7.6 Hz, 4H), 1.55 -0.58 (m, 88H).

Compound 1-3: Compound 3-2 was synthesized by Stille coupling reaction. Add trimethyl (6-undecylthieno[3,2-b]thiophen-2-yl)stantane (383 mg, 0.84 mmol) to a toluene (30 mL) solution of compounds 1-2 (300 mg, 0.28 mmol) in one portion. Heat the mixture solution to 110 ° C in a nitrogen atmosphere for 20 hours. After cooling to room temperature, wash with saturated salt water and dichloromethane. Remove solvent under reduced pressure. Subsequently, the crude product was purified by silica gel column chromatography to obtain yellow oily solid compound 1-3 (200 mg, 75% yield). ^{1}H NMR (400 MHz, $CDCl_3$) δ 9.53 (s, 2H), 8.53 (d, J = 8.4 Hz, 2H), 7.94 (d, J = 8.5 Hz, 4H), 7.66 (d, J = 6.2 Hz, 2H), 7.16 - 6.96 (m, 4H), 4.71 (d, J = 7.6 Hz, 4H), 2.76 (d, J = 7.6 Hz, 6H), 1.65- 0.58 (m, 132H).

Compound 1-4：Compounds 1-3 (200 mg; 0.2 mmol) were dissolved into 1,2-dichloroethane (20 ml) in a three-neck flask. The solution was flushed with nitrogen in 0°C for 30 min. Then, add $POCl_3$ (0.25 mL) and DMF (0.25 mL) to the solution, then let the solution temperature return to room temperature for 1h. Next, the solution was reacted at 85 °C for 16 h under nitrogen protection. After that the mixture was poured into ice water (50 mL), neutralized with aqueous AcONa. Washed with saturated salt water and dichloromethane. The solvent was removed under reduced pressure. The crude product was subsequently purified by column chromatography on silica gel to afford compound 1-4 as orange solid (180mg, 90% yield). ^{1}H NMR (400 MHz, $CDCl_3$) δ 10.18 (s, 4H), 7.97 (d, *J* = 7.8 Hz, 4H), 7.64 (d, *J* = 6.4 Hz, 4H), 6.90 (s, 2H),3.60 (t, *J* = 7.6 Hz, 4H), 2.01-1.91 (m, 4H), 1.45-0.64 (m, 134H).

FQx-IC: INCN-2F (230 mg, 1 mmol) and compound 1-4 (180 mg, 0.18 mmol) were added to a solvent mixture of chloroform (20 mL). After 0.8mL pyridine were added, the mixture was stirred at 65°C overnight. After cooling to room temperature, the reaction mixture was poured into water and extracted several times with chloroform. Removed solvent by reduced pressure and the residue was purified on a silica-gel column chromatography using chloroform as eluent to give FQx-IC as blue solid. (200mg, 90%yield)^{1}H NMR (400 MHz, $CDCl_3$) δ 8.98 (d, *J* = 33.3 Hz, 6H), 8.48 (s, 4H), 8.06-7.36 (m, 12H), 5.02 (s, 4H), 3.20 (d, *J* = 38.3 Hz, 8H). 2.50-0.5(m, 130H).

Compound 2-2: Compound 2-2 was synthesized by similar procedure as compound 1-2 between compound 2-1 and compound 2-(4-bromophenyl)-2-oxoacetaldehyde. The final product was obtained as yellow solid (300 mg, 50% yield). ^{1}H NMR (400 MHz, $CDCl_3$) δ8.70 (s, 1H), 8.49 (d, *J* = 4.6 Hz, 2H), 7.53 (d, *J* = 4.2 Hz, 2H), 6.90 (s, 2H), 4.03 (d, *J* = 8.2 Hz, 4H), 2.68 (t, *J* = 8 Hz, 4H), 1.93 (m, 2H), 1.26-0.77 (m, 118H)

Compound 2-3: Compound 2-3 was synthesized by similar procedure as compound 1-3 between compound 2-2 and compound trimethyl (6-undecylthieno [3,2-b] thiophen-2-yl) stantane. The final product was obtained as yellow solid (200 mg, 75% yield).^{1}H NMR (400 MHz, $CDCl_3$) δ 9.53 (s, 1H), 8.53 (d, *J* = 8.4 Hz, 2H), 7.94 (d, *J* = 8.5 Hz,

1H), 7.66 (d, *J* = 6.2 Hz, 1H), 7.14-6.94 (m, 2H), 4.71 (d, *J* = 7.6 Hz, 2H), 2.83 (dd, *J* = 15.6, 11.8, 6.4 Hz, 6H). 1.93 (m, 2H), 2.26-0.77 (m, 143H)

Compound 2-4: Compound 2-4 was synthesized by similar procedure as compound 1-4 with compound 2-3. The final product was obtained as orange solid (220 mg, 90% yield). ^{1}H NMR (400 MHz, $CDCl_3$) δ 10.32-9.97 (m, 3H), 9.52 (s, 1H), 8.52 (d, *J* = 8.2 Hz, 2H), 7.97 (d, *J* = 8.3 Hz, 2H), 7.69 (s, 1H), 4.73 (d, *J* = 6.4 Hz, 4H), 3.24 (ddd, *J* = 26.7, 15.6, 7.5 Hz, 6H). 1.80-0.55(m, 141H).

TQx-IC: Compound TQx-IC was synthesized by similar procedure as FQx-IC between compound 2-4 and INCN-2F. The final product was obtained as black solid (200 mg, 85% yield).^{1}H NMR (400 MHz, $CDCl_3$)δ 9.22 (s, 1H), 9.08-8.88 (m, 3H), 8.65 -8.47 (m, 1H), 8.37 (dd, *J* = 19.9, 9.9 Hz, 2H), 7.98 (s, 2H), 7.83 (t, *J* = 7.4 Hz, 1H), 7.73 (t, *J* = 7.5 Hz, 1H), 7.59 (dd, *J* = 15.7, 8.1 Hz, 3H), 4.93 (d, *J* = 11.3 Hz, 4H), 3.28 -2.96 (m, 6H), 2.61-2.16 (m, 4H), 1.50-0.67(m, 136H).

2. Experimental

Materials and synthesis

Solvents and other common reagents were obtained from Beijing Chemical Plant. All other chemicals were purchased from commercial sources (Alfa, Acros, TCI, J&K, and Sigma–Aldrich) and used without further purification unless otherwise stated. PM6 was purchased from Solarmer Materials Inc. The detailed synthetic procedures of FQx-IC, TQx-IC and the corresponding structural characterizations can be found in the Supplementary information.

Device fabrication

The OSCs devices were fabricated with conventional device structure of ITO/PEDOT:PSS/active layer/PNDIT-F3N/Ag. The PEDOT:PSS solution was spin coated on top of the cleaned ITO-coated glass substrate and the PEDOT:PSS film thickness was approximately 30 nm. After thermal annealing for 15 minutes at 150 ℃.

The blended solution was prepared by mixing donors and acceptor in a weight ratio into chloroform (CF) with the addition of a small amount of 1,8-diiodooctane. Subsequently, the active layer was spin-coated from blend chloroform solutions with a rotation speed in 3000-3500 r/min. After thermal annealing at 100℃ for 10 min, a concentration of 0.5 mg/ml PNDIT-F3N with a small amount of acetic acid spin-coated on the active layer with a rotation speed of 3000 r/min. Finally, a layer of ~100 nm Ag layer was evaporated under a high vacuum (<1 × 10^{-4} Pa).

Measurements and instruments

Mass spectra were determined on a Bruker microflex MALDI-TOF mass spectrometer. ^{1}H NMR was obtained on a Bruker Avance 400 NMR spectrometer using tetramethylsilane as an internal standard. The geometry structures of three acceptors were optimized by using DFT calculations (B3LYP/6-31G(d, p)) and all calculations were carried out using Gaussian 09. Ultraviolet-visible (UV−vis) spectra was obtained with a Perkin Elmer Lambda 950 spectrophotometer. Electrochemical cyclic voltammetry was conducted on a CHI 760E workstation with Pt plate coated with the small molecule film, Pt plate, and Ag/Ag^{+} electrode as the working electrode, counter electrode, and reference electrode, respectively, in a 0.1 mol/L tetrabutylammonium hexafluorophosphate (Bu_4NPF_6) acetonitrile solution. Ag/Ag^{+} electrode potentials were calibrated with the ferrocene/ferrocenium (Fc/Fc^{+}) redox couple (−4.8 eV relative to the vacuum level). Contact angle (θ) in solutions of PM6, FQx-IC and TQx-IC are measured on ITO/glass substrate by using the pendant drop method with the XG-CAMB3 standard contact angle meter. The calculation of surface tension by DCA (dynamic contact angle). The Flory-Huggins interaction parameter can be written as the formula below:

$$\chi_{ij} = \mathrm{K}\left(\sqrt{\gamma_i} - \sqrt{\gamma_j}\right)$$

Where K is a positive constant, where γ_i and γ_j are the surface energy of the donor and acceptor materials, respectively. The current density–voltage (*J–V*) characteristics were collected using a Keithley 2400 Source under an AM 1.5G spectrum from a solar

simulator. Light intensity is calibrated with a Newport Oriel PN 91150V Si -based solar cell. The effective area of the device is 0.04 cm^2. The EQE measurements of the devices were performed in air with an Oriel Newport system (Model 66902) equipped with a standard Si diode. Monochromatic light was generated from a Newport 300 W lamp source. The thickness of the active layer was measured on a Kla-TencorAlpha-StepD-120 Stylus Profiler. EQE_{EL} measurements were performed by applying external voltage/current sources through the devices (ELCT-3010, Enlitech). The electron mobility was acquired with the device structure of Al/Active layer /PNDIT-F3N-Br/Al, the hole mobility was obtained by preparing the structure of ITO/PEDOT:PSS/active layer/MoO_x/Ag. *J–V* characteristics were measured in the range of 0-5 V using a Keithley 2400source-measure unit in the dark. For the fitting, an SCLC model was used mathematically expressed as:

$$J = \frac{9}{8}\varepsilon_0\varepsilon_r\mu_0\frac{(V - V_{bi})^2}{L^3}exp(0.89\gamma\sqrt{\frac{V - V_{bi}}{L}})$$

Where ε_0, ε_r is the dielectric constant of the semiconductor layer, μ_0 is the zero-field mobility, V_{bi} is the built-in potential due to the anode-cathode work function offset, L is the thickness of the active layer, and γ is the field-dependence coefficient. EQE_{EL} measurements were performed by applying external voltage/current sources through the devices (ELCT-3010, Enlitech). The E_{loss} in organic solar cells can be divided into three parts as follows:

$$E_{loss} = E_g^{pv} - qV_{OC}$$

$$= \left(E_g^{pv} - qV_{OC}^{SQ}\right) + \left(qV_{OC}^{SQ} - qV_{OC}^{rad}\right) + (qV_{OC}^{rad} - qV_{OC})$$

$$= \left(E_g^{pv} - qV_{OC}^{SQ}\right) + qV_{OC}^{rad,\,below\,gap} + qV_{OC}^{non-rad}$$

$$= q\Delta V_1 + q\Delta V_2 + q\Delta V_3$$

$$= \Delta E_1 + \Delta E_2 + \Delta E_3$$

In this formula, q is the elementary charge; $VSQ\ OC$ is the maximum voltage in the Shockley–Queisser (SQ) limit model, and $V\mathrm{rad}\ OC$ is the open-circuit voltage with only radiative recombination in the device. Transmission electron microscopy (TEM) images were acquired on Tecnai G2 F20 U-TWIN TEM instrument. The atomic force microscopy (AFM) characterization was performed by Bruker Multimode 8 in Scan Asyst Mode in air. Grazing incidence wide angle X-ray scattering (GIWAXs) measurement was conducted at the beamline of 7.3.3 at the Advanced Light Source (ALS). The measurement details of in-situ UV-vis: a specially designed spin coater, which allows a detective beam to pass through the center of the fabricating devices, was applied to measure the in-situ UV-vis spectrum. An F-20 spectrometer from filmetrics was used to record the spectrum, and the time revolution of the spectrum was 5 ms. Firstly, the ITO glass substrate with PEDOT:PSS is placed onto the spin coater, the probe beam from the spectrometer passes through the substrate to the detector at the bottom of the spin coating machine. Absorption baseline was taken with substrate before each coating session. Secondly, the same spin coat procedure for device fabrication is conducted, while the spectrometer records the absorption spectrum changes over time. The sampling interval of the spectrometer is set to 4 ms. Finally, stop recording data after detecting no spectral changes, and the test ends.

Detailed Analysis

Charge mobilities: The hole mobilities (μ_h) and electron mobilities (μ_e) are estimated. The *J-V* curves of hole-only and electron-only devices were shown in Fig. S9. D18:FQx-IC blend film exhibited the μ_h/μ_e of $3.51\times10^{-4}/2.48\times10^{-4}$ $cm^2\ V^{-1}\ s^{-1}$, whereas D18:TQx-IC blend film showed higher μ_h/μ_e of $5.25\times10^{-4}/4.56\times10^{-4}$ $cm^2\ V^{-1}\ s^{-1}$, leading to much balanced μ_h/μ_e ratio of 1.15 than D18:FQx-IC-based devices (1.41) (Table S6). This may be related to the increased intramolecular interactions and crystalline caused by stronger planarity of TQx-IC.

Energy loss: The E_{loss} values were calculated to be 0.525, and 0.512 for D18:FQx-IC, and D18:TQx-IC-based devices, and other resulting E_{loss} parameters were

summarized in Fig. 2h, 2i and Table S8. The two systems showed negligible differences in ΔE_1 and ΔE_3, while the various ΔE_2s lead to different E_{loss}. The energy level difference between TQx-IC and donor D18 is smaller, resulting in lower energy loss and higher V_{OC} in the device. This result has certain guiding that we can adopt multi arm acceptors with higher LUMO energies to control the E_{loss} and to improve device performance without sacrificing V_{OC}.

Situ-absorption: From a macro perspective, FQx-IC blend films showed a slower film-forming process, which explains the oversized phase separation scale and poor exciton separation properties. As illustrated in Fig. 4b and Fig. 4e, the changes in the main peak of the two systems exhibited enormous differences. Based on the spectral evolution, the intensity and position changes of the two peaks were fitted and plotted using the Grow-Move Two Peak Model (Fig. 4g and 4h). It can be seen that the ratio of the intensity of the moving peaks in the TQx-IC blend film is significantly higher than that in the FQx-IC blend film.

3. Figures

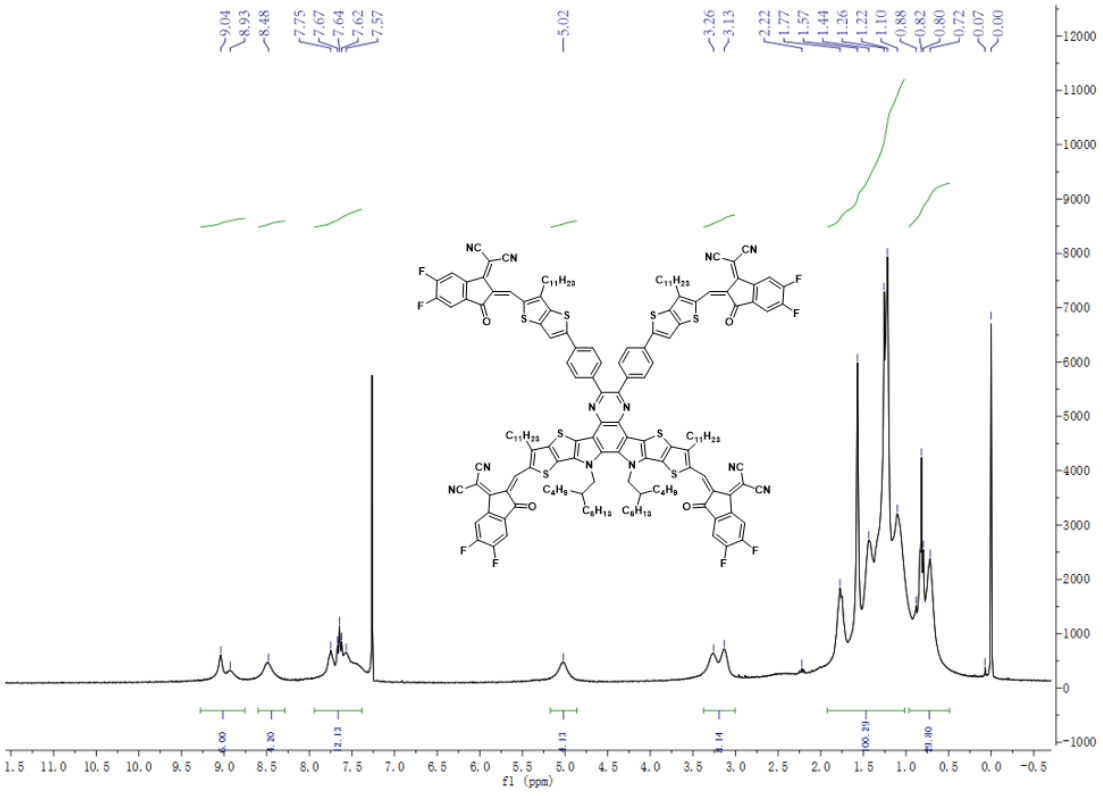

Fig. S1 ^{1}H NMR spectrum of FQx-IC.

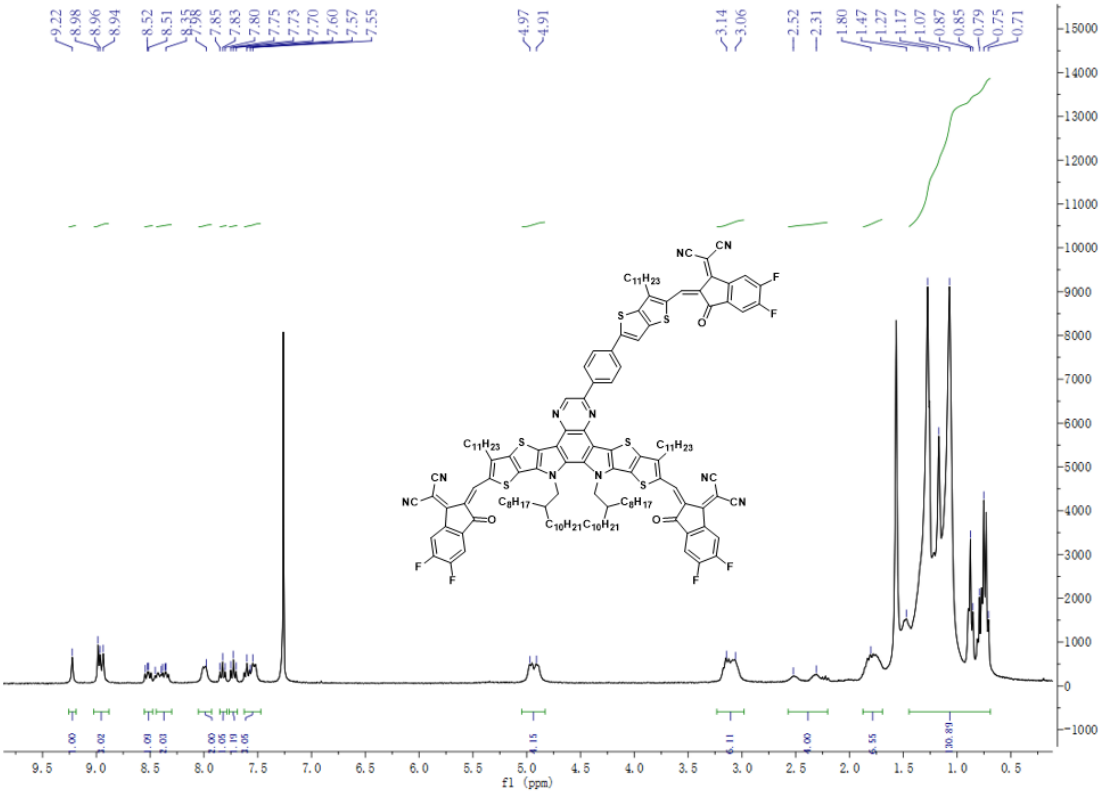

Fig. S2 ^{1}H NMR spectrum of TQx-IC.

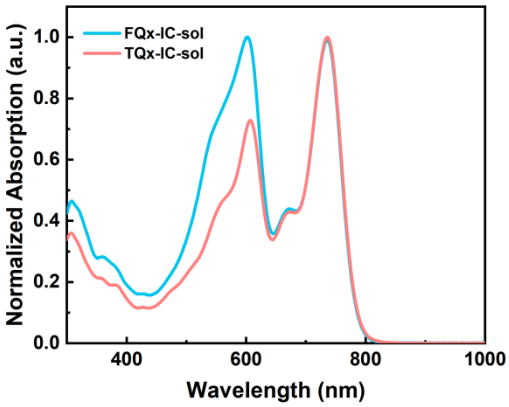

Fig. S3 Solution absorption spectra of FQx-IC and TQx-IC.

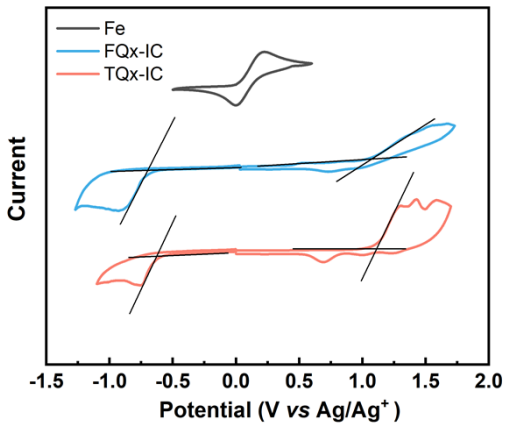

Fig. S4 Cyclic voltammogram for the two acceptors.

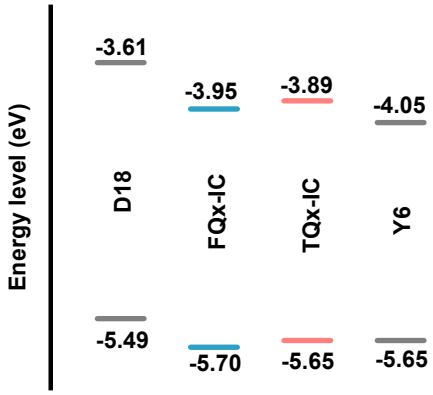

Fig. S5 Energy levels of D18, FQx-IC, TQx-IC, and Y6.

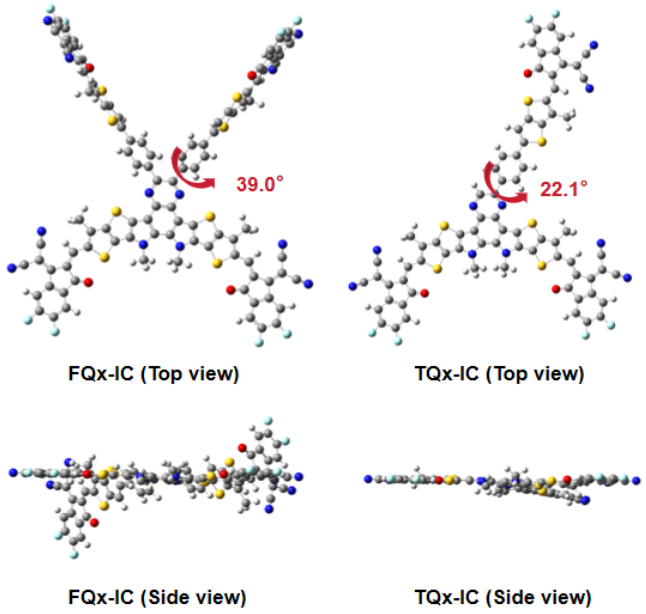

Fig. S6 Optimal conformation simulated by DFT calculations for FQx-IC and TQx-IC in simplified modes (top view and side view).

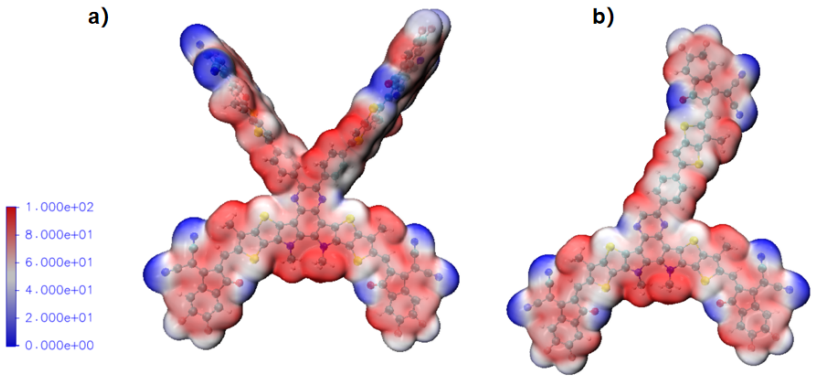

Fig. S7 Electrostatic surface potential (ESP) maps for (a) FQx-IC, and (b) TQx-IC.

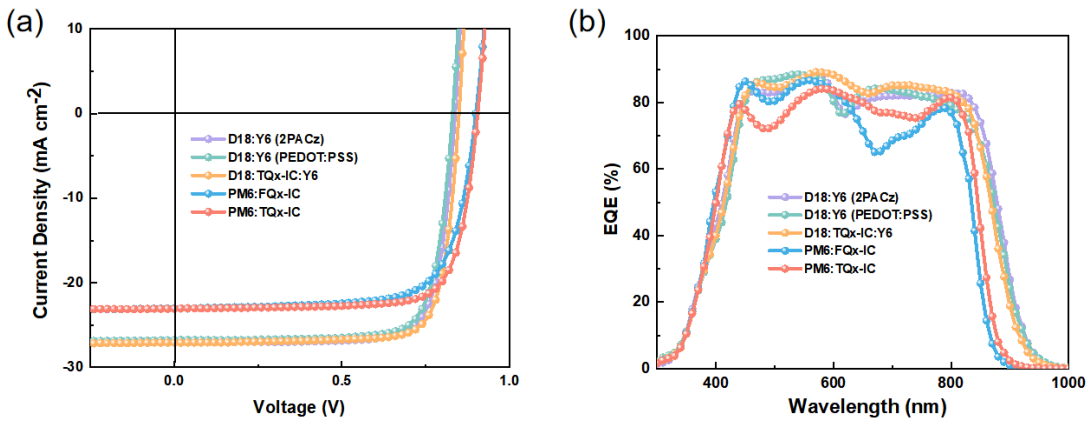

Fig. S8 (a) *J*-*V* curve and (b) EQE curve of above devices.

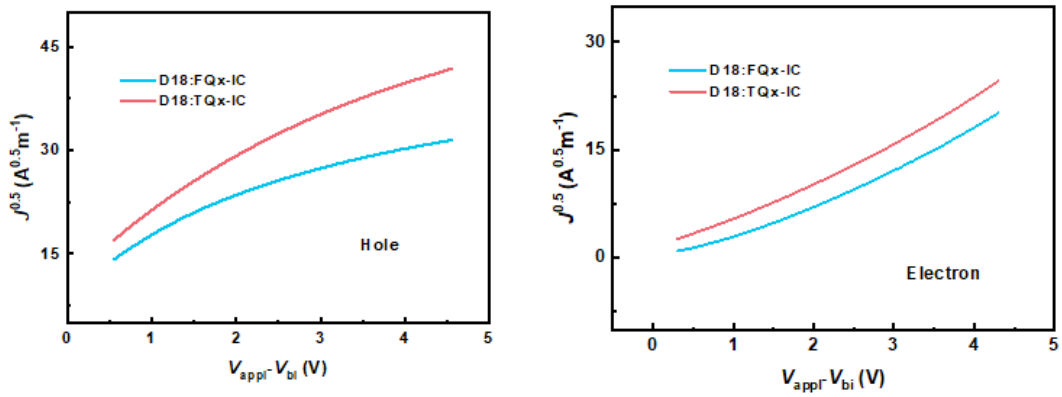

Fig. S9 $J^{0.5}$~V characteristics of the charge carrier mobility measurements of devices.

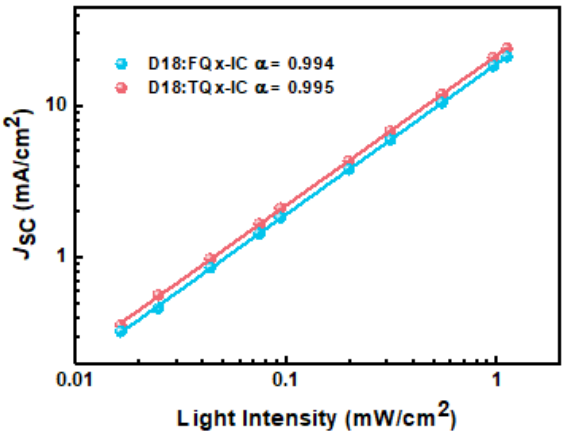

Fig. S10 Light intensity dependence of J_{SC} values of the corresponding device.

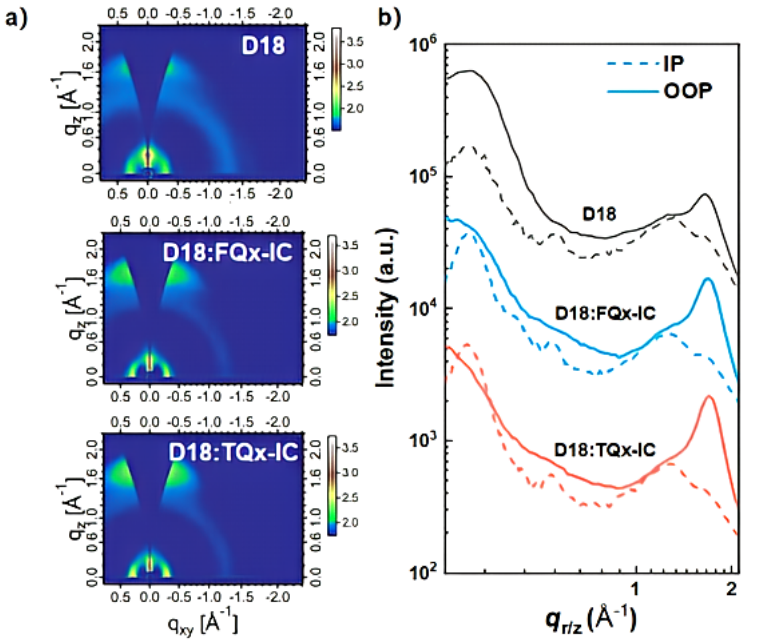

Fig. S11 (a) In-plane (solid lines) and out-of-plane (dashed lines) cuts of films; (b)Two- dimensional GIWAXS patterns of films

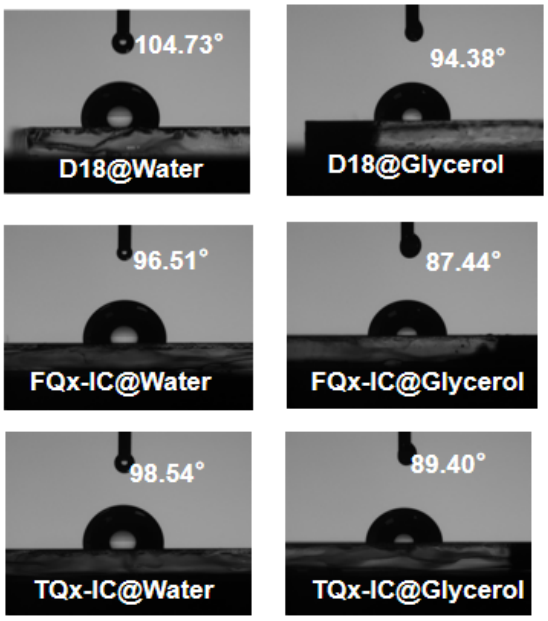

Fig. S12 The images of water and glycerol drops on neat films.

4. Tables

Table S1 Optical parameters and energy levels of FQx-IC and TQx-IC.

Acceptors	λ_{max} (nm) solution	λ_{max} (nm) film	λ_{onset} (nm) film	E^{opt}_{g} (eV)	E_{HOMO} (eV)	E_{LUMO} (eV)	ε_{film} (cm^{-1})
FQx-IC	735	778	855	1.45	-5.70	-3.95	1.21×10^5
TQx-IC	735	786	861	1.44	-5.65	-3.89	1.10×10^5

Table S2 Device optimization for D18:FQx-IC blends.

D: A	Additives	Thermal annealing	V_{OC} (V)	J_{SC} ($mA\cdot cm^{-2}$)	FF (%)	PCE (%)
1:1.2	/	80 ℃, 3 min	0.942	22.31	76.28	16.03
1:1.4	/	80 ℃, 3 min	0.940	22.46	76.12	16.07
1:1.2	10 mg/mL DIB	80 ℃, 3min	0.943	22.97	74.98	16.24
1:1.3	10 mg/mL DIB	80 ℃, 3 min	0.948	22.22	76.73	16.16
1:1.4	10 mg/mL DIB	80 ℃, 3 min	0.945	22.05	75.18	15.67
1:1.5	10 mg/mL DIB	80 ℃, 3 min	0.926	24.84	70.25	16.16
1:1.2	10 mg/mL DIB	/	0.939	22.19	74.98	15.62
1:1.2	10 mg/mL DIB	100 ℃, 3 min	0.922	22.34	74.98	15.45

Table S3 Device optimization for D18:TQx-IC blends.

D: A	Additives	Thermal annealing	V_{OC} (V)	J_{SC} (mA·cm^{-2})	FF (%)	PCE (%)
1:1.2	/	80 ℃, 3 min	0.950	24.14	74.64	17.12
1:1.4	/	80 ℃, 3 min	0.948	24.03	74.11	16.88
1:1.2	10 mg/mL DIB	80 ℃, 3min	0.950	24.07	74.59	17.06
1:1.3	10 mg/mL DIB	80 ℃, 3 min	0.950	24.10	75.15	17.20
1:1.4	10 mg/mL DIB	80 ℃, 3 min	0.948	24.41	73.76	17.06
1:1.5	10 mg/mL DIB	80 ℃, 3 min	0.927	24.83	72.99	16.81
1:1.2	10 mg/mL DIB	/	0.949	24.37	75.06	17.36
1:1.2	10 mg/mL DIB	100 ℃, 3 min	0.946	23.40	75.21	16.65

Table S4 Device optimization for D18:Y6:TQx-IC blends.

D: A	Additives	Thermal annealing	V_{OC} (V)	J_{SC} (mA·cm^{-2})	FF (%)	PCE (%)
1:1.1:0.1	/	80 ℃, 3 min	0.840	26.91	80.57	17.66
1:1:0.2	/	80 ℃, 3 min	0.846	24.56	79.44	18.02
1:1.1:0.1	10 mg/mL DIB	80 ℃, 3min	0.844	15.37	80.03	18.25
1:1:0.2	10 mg/mL DIB	80 ℃, 3 min	0.850	27.53	80.43	18.82
1:0.9:0.3	10 mg/mL DIB	80 ℃, 3 min	0.864	25.83	78.88	17.60
1:0.8:0.4	10 mg/mL DIB	80 ℃, 3 min	0.873	25.53	80.66	17.98
1:1:0.2	10 mg/mL DIB	/	0.846	26.91	80.66	18.30
1:1:0.2	10 mg/mL DIB	100 ℃, 3 min	0.849	26.57	80.03	18.41

Table S5 Device performances of the related systems. The average values and standard deviations were obtained from 8 devices.

Active Layer	Transport Layer	V_{OC} (V)	J_{SC} (mA·cm^{-2})	FF (%)	PCE (%)
D18:Y6	2PACz	0.838	27.02	79.31	17.96 (17.88±0.32)
D18:Y6	PEDOT:PSS	0.830	26.79	78.68	17.50 (17.37±0.16)
D18:TQx-IC:Y6	PEDOT:PSS	0.849	27.08	80.03	18.41 (18.30±0.19)
PM6:FQx-IC	PEDOT:PSS	0.900	23.03	72.87	15.10 (14.98±0.21)
PM6:TQx-IC	PEDOT:PSS	0.905	23.06	77.39	16.15 (16.02±0.17)

Table S6 The electron mobility (μ_e)/hole mobility (μ_h) values of the blend films.

Active layer	μ_h (cm^2·V^{-1}·s^{-1})	μ_e (cm^2·V^{-1}·s^{-1})	μ_h/μ_e
D18:FQx-IC	3.51×10^{-4}	2.48×10^{-4}	1.41
D18:TQx-IC	5.25×10^{-4}	4.56×10^{-4}	1.15

Table S7 Charge carrier transport parameters of the optimized devices.

Devices	$J_{ph(a)}$ (mA·cm^2)	$J_{ph(b)}$ (mA·cm^2)	J_{sat} (mA·cm^2)	η_{diss} (%)	η_{coll} (%)
D18:FQx-IC	19.98	19.54	21.24	94.06	91.99
D18:TQx-IC	22.10	21.54	22.37	98.79	96.29

(a The photocurrent density obtained under the maximum output power of the device)

(b The photocurrent density obtained under the short-circuit state of the device)

Table S8 Detailed E_{loss} of the devices.

Devices	E_g^{pv} (eV)	EQE_{EL}	qV_{OC}^{SQ} (eV)	qV_{OC}^{rad} (eV)	E_{loss} (eV)	ΔE_1 (eV)	ΔE_2 (eV)	ΔE_3 (eV)
D18:FQx-IC	1.480	3.14×10^{-4}	1.214	1.163	0.525	0.265	0.051	0.209
D18:TQx-IC	1.476	2.79×10^{-4}	1.209	1.177	0.512	0.267	0.033	0.212

Table S9 GIWAXS measurement parameters of the related films.

Films		q (Å^{-1})	d-spacing (Å)	FWHM (Å^{-1})	CCL (Å)
D18	OOP(010)	1.65	3.80	0.348	18.04
FQx-IC		1.67	3.76	0.237	26.51
TQx-IC		1.70	3.69	0.298	21.08
D18:FQx-IC	OOP(010)	1.69	3.72	0.258	24.35
D18:TQx-IC		1.70	3.69	0.240	26.18

Acceptors	$\gamma^{accepter}$ (mN/m^2)	Donor	γ^{donor} (mN/m^2)	χ
FQx-IC	14.34	D18	10.48	0.30
TQx-IC	13.26	D18	10.48	0.16

Table S10 The parameters of surface energies.